

# Synchrotron X-ray microfluorescence measurement of metal distributions in *Phragmites australis* root system in the Yangtze River intertidal zone

Huan Feng,<sup>a\*</sup> Weiguo Zhang,<sup>b</sup> Yu Qian,<sup>a‡</sup> Wenliang Liu,<sup>b</sup> Lizhong Yu,<sup>b</sup> Shinjae Yoo,<sup>c</sup> Jun Wang,<sup>d</sup> Jia-Jun Wang,<sup>d</sup> Christopher Eng,<sup>d</sup> Chang-Jun Liu<sup>e</sup> and Ryan Tappero<sup>d</sup>

Received 13 January 2016

Accepted 18 May 2016

Edited by S. M. Heald, Argonne National Laboratory, USA

‡ Current address: School of Ecology and Environmental Sciences, Yunnan University, Kunming, Yunnan 650091, People's Republic of China.

**Keywords:** Yangtze River intertidal zone; metal uptake; *Phragmites australis*; Fe nanoparticles.

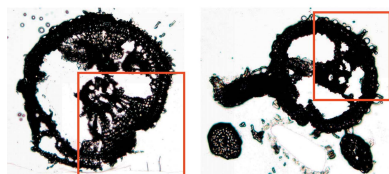
<sup>a</sup>Department of Earth and Environmental Studies, Montclair State University, Montclair, NJ 07043, USA, <sup>b</sup>State Key Laboratory of Estuarine and Coastal Research, East China Normal University, Shanghai 200062, People's Republic of China, <sup>c</sup>Computational Science Center, Brookhaven National Laboratory, Upton, NY 11973, USA, <sup>d</sup>Photon Sciences Directorate, Brookhaven National Laboratory, Upton, NY 11973, USA, and <sup>e</sup>Biological Sciences Department, Brookhaven National Laboratory, Upton, NY 11973, USA. \*Correspondence e-mail: fengh@mail.montclair.edu

This study investigates the distributions of Br, Ca, Cl, Cr, Cu, K, Fe, Mn, Pb, Ti, V and Zn in *Phragmites australis* root system and the function of Fe nanoparticles in scavenging metals in the root epidermis using synchrotron X-ray microfluorescence, synchrotron transmission X-ray microscope measurement and synchrotron X-ray absorption near-edge structure techniques. The purpose of this study is to understand the mobility of metals in wetland plant root systems after their uptake from rhizosphere soils. *Phragmites australis* samples were collected in the Yangtze River intertidal zone in July 2013. The results indicate that Fe nanoparticles are present in the root epidermis and that other metals correlate significantly with Fe, suggesting that Fe nanoparticles play an important role in metal scavenging in the epidermis.

## 1. Introduction

A wetland plant root system is an active site for transport of oxygen into the soil/sediment and absorption of water and nutrients in solution even against a concentration gradient (Enstone *et al.*, 2002). Many plants acquire metals from the rhizosphere and regulate their uptake properties within the root system (Hinsinger & Courchesne, 2008). Although the metal availability in the sediments is the source for plant uptake, metal properties and plant species are also factors affecting the metal transport in the plants. Other factors which complicate the synergistic interactions with the environmental parameters are factors such as soil pH, redox potential ( $E_h$ ), water availability, microbes and other biota, and mineral and organic content (Hinsinger & Courchesne, 2008; Morrissey & Gueriot, 2009).

Natural processes that control the mobility of metals in soils and plants determine the biogeochemical cycle of trace elements. Because metals in the plant tissues are originated from the rhizosphere through root system absorption, investigation of metal uptake mechanisms, transport processes and the function of Fe plaque controlling the metal mobility in plant root systems are important and informative in understanding metal translocation and the biogeochemical cycle in wetlands. In the rhizosphere, the role of Fe plaque, which forms on the surface of plant roots, in controlling the metal biochemical cycle has been an issue of debate. Several early studies suggest that Fe plaque serves as a barrier preventing



heavy metals from entering plant roots (St-Cyr & Campbell, 1996; Bjørn *et al.*, 1998). However, others suggest that Fe plaque is not the main barrier (Ye *et al.*, 1998; Liu *et al.*, 2004). The Yangtze River estuary is one of the world's largest estuarine systems and is defined as a mesotidal estuary. Huge amounts of sediment ( $\sim 4.86 \times 10^8$  ton  $y^{-1}$  during 1949–1984) are discharged from the Yangtze River annually, resulting in an extensive intertidal zone in the Yangtze River estuary (Xiqing, 1998). The river's intertidal zone typically contains three distinct vegetation units seaward: a *Phragmites australis* zone, a *Scirpus mariqueter* and *Scirpus trigueter* zone, and bare unvegetated mudflats (Zhang *et al.*, 2001). *Spartina alterfloria* became a predominant species in the area after it was planted in the 1990s for promotion of sediment accretion and coastal defense.

Previous studies have shown that wetland plants can absorb metals from the soils and store these metals in the plant biomass (Williams *et al.*, 1994; Weis & Weis, 2004; Gallagher *et al.*, 2008; Qian *et al.*, 2012). Freshwater wetland plants may exhibit metal uptake and transport behaviors that are different from saltwater wetland plants; however, these behaviors may also vary between species within their respective categories. Recently, several studies have indicated the presence of the Fe nanocomplexes or Fe nanoparticles in root cross-sections (Pardha-Saradhi *et al.*, 2014; Fuente *et al.*, 2016). In general, these Fe nanoparticles are amorphous iron oxyhydroxide and can further form larger nanocomplexes (Pardha-Saradhi *et al.*, 2014). For example, *Imperata cylindrica* (L.) P. Beauv. is a hyperaccumulator plant. It was found that Fe deposited in the form of nanocrystals, not only in the intercellular space but also in the cells of the xylem, phloem and in the epidermal cells in root rhizomes and leaves (Rodríguez *et al.*, 2005; Fuente *et al.*, 2016). These iron nanocrystals are composed of jarosite, ferrihydrite, hematite and spinel phases (Fuente *et al.*, 2016). In this study, as synchrotron X-ray diffraction (XRD) measurements were not conducted on the samples here, there is no Fe-containing mineral information that can be reported. Nevertheless, synchrotron X-ray microbeam techniques, such as synchrotron X-ray fluorescence (XRF), have important applications in studying metal translocation and accumulation in plants with micrometer-scale resolution (Martin *et al.*, 2001, 2006; Naftel *et al.*, 2001; Sutton *et al.*, 2002; Zimmer *et al.*, 2011; Feng *et al.*, 2013, 2015, 2016; Rouff *et al.*, 2013). Unlike conventional wet chemical analyses, the synchrotron-based techniques have demonstrated advantages in sample preparation and measurement. The high-spatial-resolution measurement provides high detection sensitivity and resolution of elemental distributions and leads to a better understanding of the chemical reaction mechanisms and fate of elements in the plants. This study aims at improving our current knowledge of metal uptake and accumulation in wetland plant roots using synchrotron radiation measurements for better understanding the ecological function of wetland plants and the role of Fe plaque in metal transport. Wetland in the Yangtze River intertidal zone is a unique test bed for the purpose of this study.

## 2. Materials and methods

### 2.1. Sample collection and preparation

Field work for *Phragmites australis* sample collection was conducted in July 2013 at two sites (Site 1:  $31^{\circ} 34' 55.06''$  N,  $121^{\circ} 54' 10.32''$  E; Site 2:  $31^{\circ} 34' 56.45''$  N,  $121^{\circ} 54' 12.62''$  E) on the north shore of Chongming Island within the Yangtze River intertidal zone, where *Phragmites australis* was an abundant species (Fig. 1). These two sampling sites were very close to each other ( $\sim 80$  m apart). According to a previous study in this area, the metal concentrations in the sediments between these two sites were essentially the same, which were reported to be: Fe  $3.98 \pm 0.17\%$ ; Cr  $91.7 \pm 0.6$  mg  $g^{-1}$ ; Cu  $44.4 \pm 4.7$  mg  $g^{-1}$ ; Mn  $987 \pm 3$  mg  $g^{-1}$ ; Pb  $28.9 \pm 0.5$  mg  $g^{-1}$ ; Zn  $119 \pm 13$  mg  $g^{-1}$  (Zhang *et al.*, 2009). The metal concentrations (Cr, Cu, Fe, Mn, Ti, V and Zn) except Pb in the study area were within the natural background levels (Zhang *et al.*, 2009). In this study, *Phragmites australis* samples were collected along with the soils using stainless steel spades, placed into large plastic containers and then transported to our laboratory at East China Normal University for further treatment. Bulk soils were easily removed from the plants by gentle shaking; rhizosphere soils were carefully removed by hand and the trace residual soils on the roots were rinsed off with small amounts ( $< 20$  ml) of deionized water (Otte *et al.*, 1991).

During the sample preparation for synchrotron X-ray microfluorescence ( $\mu$ XRF) measurement, the fresh root samples were suspended in an optimal cutting temperature (OCT) compound that does not infiltrate the specimen, and rapidly cooled to  $-20^{\circ}\text{C}$ . Once OCT solidified, a cryotome (Cryostat CM1950, Leica Microsystems) was used to cut  $50$   $\mu\text{m}$  thin sections. The thin sections of the root samples were

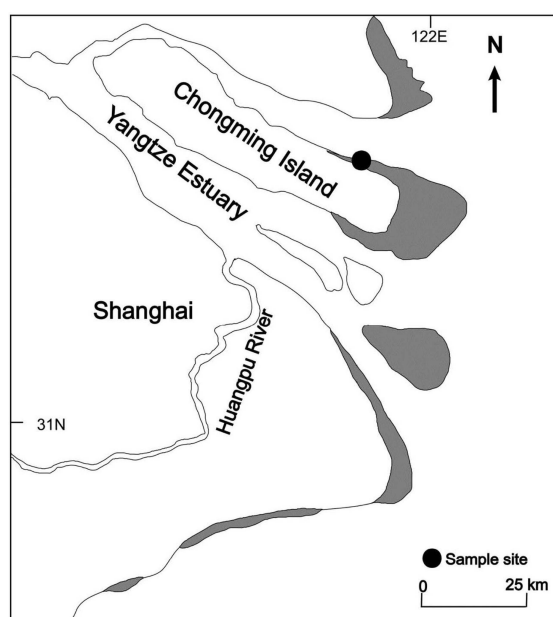


**Figure 1** Map showing the sampling sites on the north shore of Chongming Island in the Yangtze River intertidal zone.

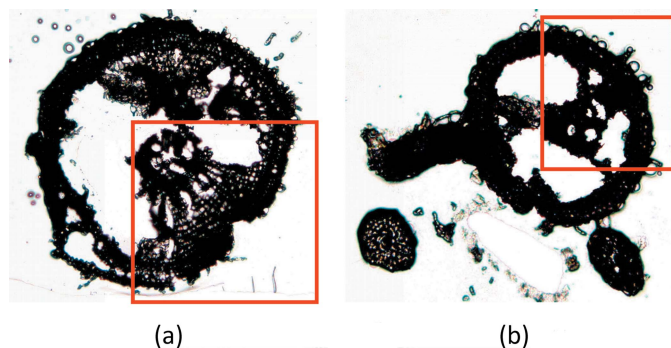


**Figure 2**  
Optical images of *Phragmites australis* root cross-section. (a) Sample 1-1 collected at Site 1. (b) Sample 2-1 collected at Site 2. The thickness of the cross sections is 50  $\mu\text{m}$ . These thin cross-section samples are prepared for synchrotron XRF measurement for metal concentrations and distributions. Areas in the frames are selected for synchrotron XRF measurement.

then mounted on 25 mm  $\times$  76 mm quartz microscope slides (SPI Supplies<sup>®</sup>) for synchrotron  $\mu\text{XRF}$  analysis (Fig. 2).

In order to examine possible differences in the root sections within the limited user time available at the beamline workstation, the root tip section of Sample 1-1 collected at Site 1 and the root basal section of Sample 2-1 collected at Site 2 were chosen for synchrotron XRF analysis. For synchrotron transmission X-ray microscope (TXM) measurement and synchrotron X-ray absorption near-edge structure (XANES) measurement to visualize Fe nanoparticles, each of the root samples was glued on the tip of a needle and then mounted on a stand (Fig. 3). All the samples prepared for synchrotron radiation measurement were kept in our low-temperature laboratory (4°C) or in a desiccator before analysis.

## 2.2. Synchrotron TXM measurement

Synchrotron TXM analysis was conducted at the National Synchrotron Light Source (NSLS) (beamline X8C at Brook-

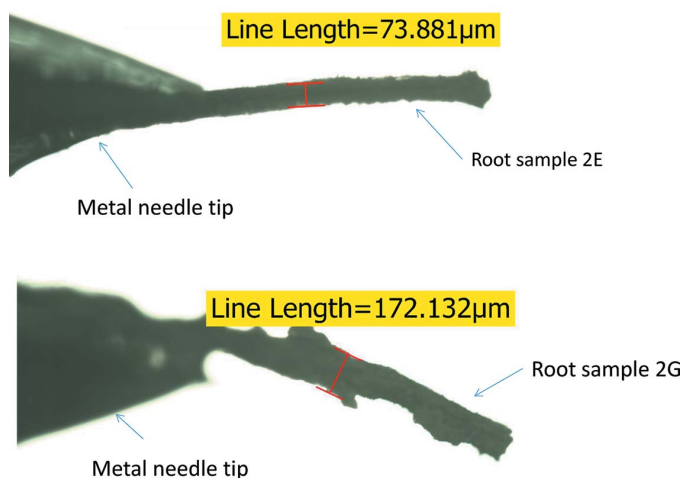


**Figure 3**  
Image of *Phragmites australis* root samples collected at Site 2 mounted on metal pin tips for synchrotron TXM measurement. Top: root sample 2E. Bottom: root sample 2G.

haven National Laboratory, Upton, NY, USA) and at the Advanced Photon Source (APS) (NSLS-II TXM transition program) at Argonne National Laboratory, Argonne, IL, USA that were equipped with a full-field TXM. The newly developed TXM provides a large field of view (40  $\mu\text{m}$   $\times$  40  $\mu\text{m}$ ), 30 nm resolution, local tomography, and automated maker-free image acquisition and alignment (Wang *et al.*, 2012, 2014a). By tuning the X-ray energy across the absorption edge of the element of interest, this TXM technique enables chemical information to be obtained with high sensitivity (Wang *et al.*, 2014b). In order to investigate the Fe distribution in the roots, XANES data were collected by scanning the X-ray energy from 7092 eV to 7192 eV with a step size of 2 eV in this study. A stack of images was obtained by scanning the photon energy across the X-ray absorption edge of elemental Fe. A lens-coupled scintillator with a 2048  $\times$  2048 pixel camera detector was used to record the images. With all 1024  $\times$  1024 pixels for binning 2  $\times$  2, the full spectrum for each pixel was extracted. The XANES analysis was carried out using a customized program (Matlab, MathWorks, R2011b) developed in-house (TXM X8C group, NSLS, BNL). Background normalization was first carried out for the TXM images with a unique background image collected at every energy. More information on TXM and XANES can be found elsewhere (Wang *et al.*, 2012, 2014b). In addition, a tomographic dataset was achieved for each sample by collecting 361 projections at a rotation range of 180° (2  $\times$  2 camera pixels with 10 s exposure time). Reconstruction and visualization of the experimental data were completed using proprietary software developed by Xradia.

## 2.3. Synchrotron X-ray fluorescence measurement

Metal concentrations and distributions in wetland plants were investigated using synchrotron  $\mu\text{XRF}$  at beamline NSLS X27A (Ablett *et al.*, 2006). Briefly, this bending-magnet beamline uses Kirkpatrick–Baez mirrors to produce a focused spot (10  $\mu\text{m}$   $\times$  10  $\mu\text{m}$ ) of hard X-rays with tunable energy achieved *via* Si(111) or Si(311) channel-cut monochromator crystals. For synchrotron  $\mu\text{XRF}$  imaging, the incident beam energy was fixed at 13.5 keV to excite all target elements simultaneously. The sample was oriented 45° to the incident beam, and rastered in the path of the beam by an XY stage while X-ray fluorescence was detected by a 13-element Canberra Ge array detector positioned 90° to the incident beam. Elemental maps were typically collected from a 1 mm<sup>2</sup> sample area using a step size of 10–20  $\mu\text{m}$  and a dwell time of 7 s. The fluorescence yields were normalized to the changes in intensity of the X-ray beam ( $I_0$ ) and the dwell time. Points of interest on the images were selected for spectroscopic analysis. During the measurement, the X-ray influences were comparatively low and radiation damage effects were minimal. Data acquisition and processing were performed using IDL-based beamline software designed by CARS (University of Chicago, Consortium for Advanced Radiation Sources) and NSLS beamline X26A. Further data analysis

was conducted at Montclair State University and Brookhaven National Laboratory.

### 2.4. Data visualization, extraction and computation

The raw data from the synchrotron radiation measurements were processed at each beamline workstation. Data visualization was achieved by IDL Virtual Machine using the software developed by CARS (University of Chicago, Consortium for Advanced Radiation Sources). Data matrix extraction of the root epidermis and vascular tissue was made possible using Matlab (MathWorks) (Fig. 4). Statistical analysis of the data was performed using Matlab (MathWorks) and Systat (Systat Software, Inc.).

## 3. Results

### 3.1. Visualization of Fe nanoparticles in root epidermis and metal distributions in root cross-section

The high-resolution Fe XANES images show that Fe is present in the root epidermis as nanoparticles (Fig. 5). The cross-section concentrations and distributions of Br, Ca, Cl, Cr, Cu, K, Fe, Mn, Pb, Ti, V and Zn in the *Phragmites australis* root samples from the epidermis to the vascular bundle are shown in Figs. 6 and 7. It can be seen that the distributions of these elements from the epidermis to the vascular bundle are apparently different. Most of these elements show very high concentrations in the epidermis, forming a nearly continuous surficial rind (Figs. 6 and 7). The average concentrations of Br, Ca, Cl, Cr, Cu, K, Fe, Mn, Pb, Ti, V and Zn in the epidermis and vascular bundle of each root collected at Sites 1 and 2 are summarized in Table 1. In general, the concentrations of these elements in the root epidermis are higher than that in the vascular bundle. This can contribute to the geochemical

reactions at the rhizosphere soil–root interface, metal uptake from the soil to the root epidermis, and concentration gradient and horizontal transport from the epidermis to vascular bundle as well as the impact of the Casparian band on metal aplastic transport. It is also seen that some localized areas in the epidermis with high Fe concentration usually have the highest metal concentrations (Figs. 6 and 7). This could be attributed to the metal co-precipitation with Fe nanoparticles. According to a previous sediment study in this area, metal concentrations between these two sites are nearly the same (Zhang *et al.*, 2009). Therefore, the concentration differences in some elements between Sample 1-1 and Sample 2-1 as shown in Table 1 may not be simply caused by the concentration differences in the sediments. Usually, the root tip is an active site for oxygen transport and nutrient uptake. For example, relatively higher metal (Ca, Cu, Fe, Mn, Pb and Zn) concentrations in new root tip than those in the main root base were found in *Spartina alterniflora* collected in the Yangtze River intertidal zone (Feng *et al.*, 2015). Therefore, although the possibility of spatial variation cannot be excluded, the difference between the root tip section and the root basal section may also cause these differences (Feng *et al.*, 2015).

### 3.2. Statistical analysis

#### 3.2.1. Mann–Whitney U non-parametric test for epidermis and vascular bundle. A Mann–Whitney U non-parametric test

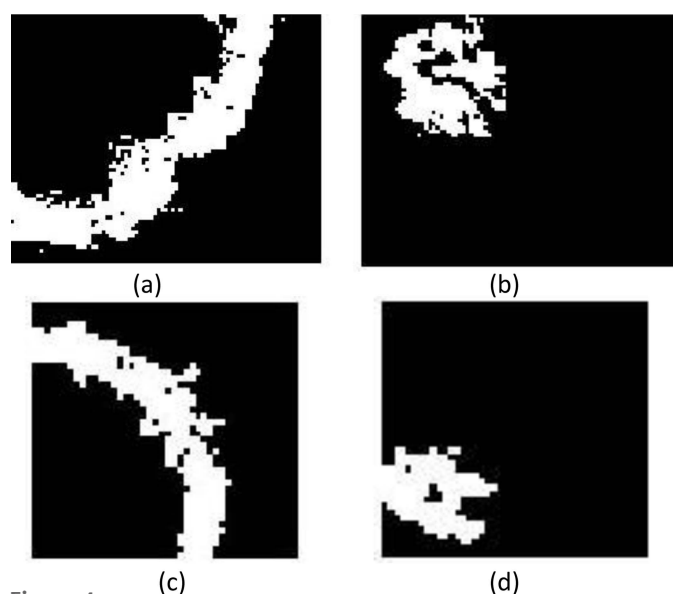


**Figure 4** Extracted areas in Sample 1-1 collected at Site 1: (a) epidermis and (b) vascular bundle; and Sample 2-1 collected at Site 2: (c) epidermis and (d) vascular bundle. Data extracted from these areas were used for the data analyses.

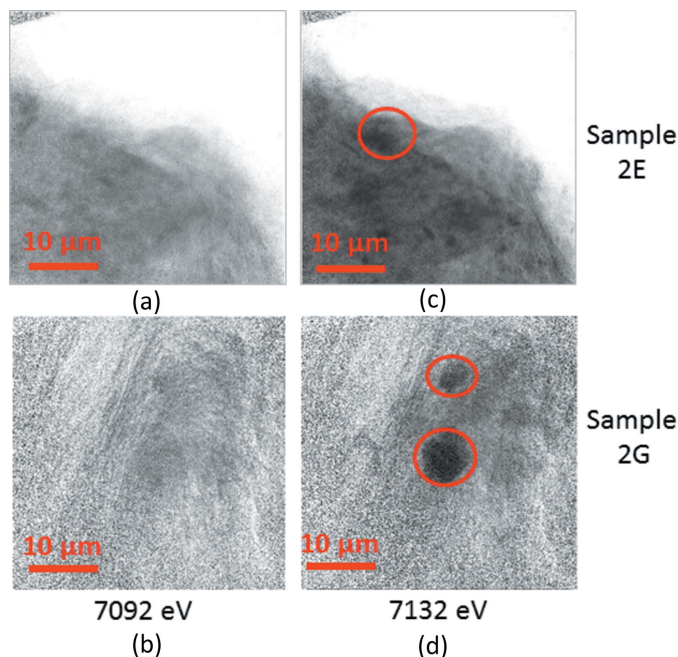


**Figure 5** Synchrotron TXM measurement for Fe XANES below and above the Fe edge on two *Phragmites australis* root samples collected at Site 2. Synchrotron XANES measurement confirms the presence of Fe nanoparticles in the epidermis of *Phragmites australis* root: (a) and (b) Fe XANES image taken at 7092 eV (below the Fe<sup>2+</sup> pre-edge); (c) and (d) Fe XANES image taken at 7132 eV (above the Fe<sup>3+</sup> pre-edge). Black dots in the circles in images (c) and (d) are Fe nanoparticles. The ‘shadows’ in (a) and (b), where Fe nanoparticles are found, indicate the absorption of other metals, such as Mn, Cu and Ni, whose pre-edges are below the Fe pre-edge. The results suggest metal scavenging by Fe nanoparticles.

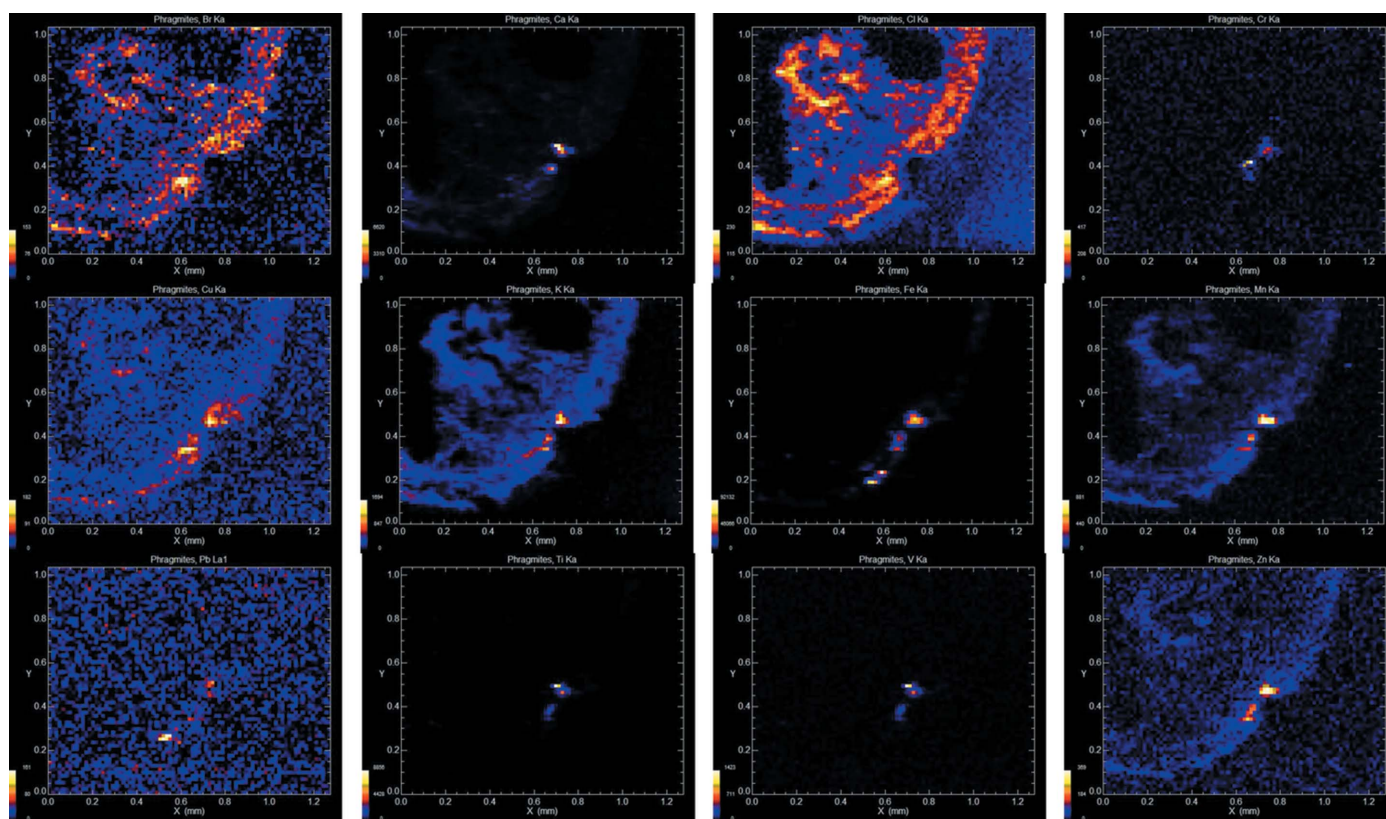
**Table 1**

Summary of Br, Ca, Cl, Cr, Cu, Fe, K, Mn, Pb, Ti, V and Zn average concentrations [mean  $\pm$  standard deviation (SD)] in units of counts per second (cps) and range of variations in the epidermis and vascular bundle in Sample 1-1 and Sample 2-1 collected at Site 1 and Site 2, respectively. Differences in the concentrations between the epidermis and the vascular tissue are element-dependent.

Sample ID	Layer	Statistics	Br	Ca	Cl	Cr	Cu	Fe
Sample 1-1	Epidermis <i>n</i> = 1237	Mean $\pm$ SD Range	41.1 $\pm$ 27.3 –44.2–154	196 $\pm$ 388 14–6621	79.4 $\pm$ 28.4 5.8–223	11.9 $\pm$ 23.0 –33.1–417.0	36.8 $\pm$ 20.9 –11.6–183	1900 $\pm$ 7267 29–92133
Sample 1-1	Vascular tissue <i>n</i> = 568	Mean $\pm$ SD Range	34.3 $\pm$ 24.7 –24.2–129	92 $\pm$ 43 11–356	87.0 $\pm$ 33.4 45.1–230	8.6 $\pm$ 10.3 –28.3–38.9	29.7 $\pm$ 15.0 –11.7–93.6	113 $\pm$ 106 10–907
Sample 2-1	Epidermis <i>n</i> = 364	Mean $\pm$ SD Range	40.1 $\pm$ 21.6 –26.5–105	173 $\pm$ 257 27–4242	71.2 $\pm$ 17.6 45.1–140	10.1 $\pm$ 9.8 –17.4–45.3	29.6 $\pm$ 12.4 –2.6–92.0	1500 $\pm$ 3077 22–30495
Sample 2-1	Vascular tissue <i>n</i> = 174	Mean $\pm$ SD Range	37.9 $\pm$ 22.8 –21.1–116	149 $\pm$ 46 44–293	72.5 $\pm$ 17.5 46.0–127	7.7 $\pm$ 9.6 –19.5–29.3	26.5 $\pm$ 13.1 –13.3–61.1	84 $\pm$ 97 0–1105

Sample ID	Layer	Statistics	K	Mn	Pb	Ti	V	Zn
Sample 1-1	Epidermis <i>n</i> = 1237	Mean $\pm$ SD Range	227 $\pm$ 139 –1.5–1695	73.7 $\pm$ 75.9 –1.4–881	13.9 $\pm$ 21.2 –45.4–161	54.3 $\pm$ 379 –48.7–8857	14.5 $\pm$ 63.9 –62.0–1423	35.8 $\pm$ 34.8 –15.7–369
Sample 1-1	Vascular tissue <i>n</i> = 568	Mean $\pm$ SD Range	200 $\pm$ 91 54–527	58.2 $\pm$ 28.4 4.8–180	10.2 $\pm$ 18.5 –40.4–66.1	8.2 $\pm$ 12.5 –25.6–115	7.4 $\pm$ 10.0 –29.5–34.6	25.8 $\pm$ 15.2 –19.3–69.5
Sample 2-1	Epidermis <i>n</i> = 364	Mean $\pm$ SD Range	192 $\pm$ 58 21–379	25.1 $\pm$ 26.9 –8.8–320	9.5 $\pm$ 18.6 –34.2–78.3	40.2 $\pm$ 102 –16.4–1322	11.2 $\pm$ 18.6 –18.0–205	34.7 $\pm$ 19.6 –9.8–122
Sample 2-1	Vascular tissue <i>n</i> = 174	Mean $\pm$ SD Range	199 $\pm$ 57 47–386	17.8 $\pm$ 11.4 –11.3–46.2	8.0 $\pm$ 17.7 –42.2–53.5	13.0 $\pm$ 65.7 –12.7–838	6.2 $\pm$ 12.3 –14.6–122	26.9 $\pm$ 14.1 –2.6–62.5



**Figure 6**

Metal concentrations and distributions in the root tip cross-sections of Sample 1-1, *Phragmites australis*, collected at Site 1. Top row: Br, Ca, Cl and Cr. Second row: Cu, K, Fe and Mn. Third row: Pb, Ti, V and Zn.

Table 2

Results of Mann-Whitney U non-parametric test and two-sample *t*-test to examine metal concentration difference between the root tip and the root basal tissue. The results indicate that some elements (Ca, Cl, Cu and Mn) show significant differences ( $p < 0.001$ ), while the others show no difference.

Type of test	log (Br)	log (Ca)	log (Cl)	log (Cr)	log (Cu)	log (Fe)	log (K)	log (Mn)	log (Pb)	log (Ti)	log (V)	log (Zn)
Mann-Whitney U non-parametric test												
<i>p</i> -value	0.530	0.000	0.000	0.023	0.000	0.810	0.069	0.000	0.040	0.002	0.122	0.461
Two-sample <i>t</i> -test												
<i>p</i> -value	0.526	0.000	0.000	0.036	0.000	0.227	0.048	0.000	0.147	0.037	0.034	0.321
Bonferroni adjusted <i>p</i> -value	1.000	0.000	0.000	0.429	0.000	1.000	0.575	0.000	1.000	0.443	0.409	1.000
Dunn-Sidak adjusted <i>p</i> -value	1.000	0.000	0.000	0.354	0.000	0.955	0.445	0.000	0.852	0.363	0.340	0.990

and two-sample *t*-test were performed on these two root samples to examine the concentration differences between these two root samples and between the epidermis and the vascular bundle in each sample. Logarithmic transformation was performed on the data before the analysis to ensure a normal distribution. The results show that, except for Ca, Cl, Cu and Mn, there are no significant differences between these two samples in terms of element concentrations (Table 2). However, concentration differences between the epidermis and the vascular bundle are found in some elements in one or both of the roots (Table 3).

**3.2.2. Pearson correlation analyses.** To examine correlations between the elements (Br, Ca, Cl, Cr, Cu, K, Fe, Mn, Pb, Ti, V and Zn) in the epidermis and the vascular bundle in each root sample, Pearson correlation analysis was performed on the epidermis and vascular bundle data, respectively (Tables 4 and 5). Although the significant correlations ( $p < 0.001$ ) vary between the elements in the epidermis and the vascular bundle, respectively, the results show that these elements are in general correlated significantly with Fe in the epidermis. To examine the function of Fe in metal scavenging, we treated all the data as one entity, *i.e.* no distinction between the sampling

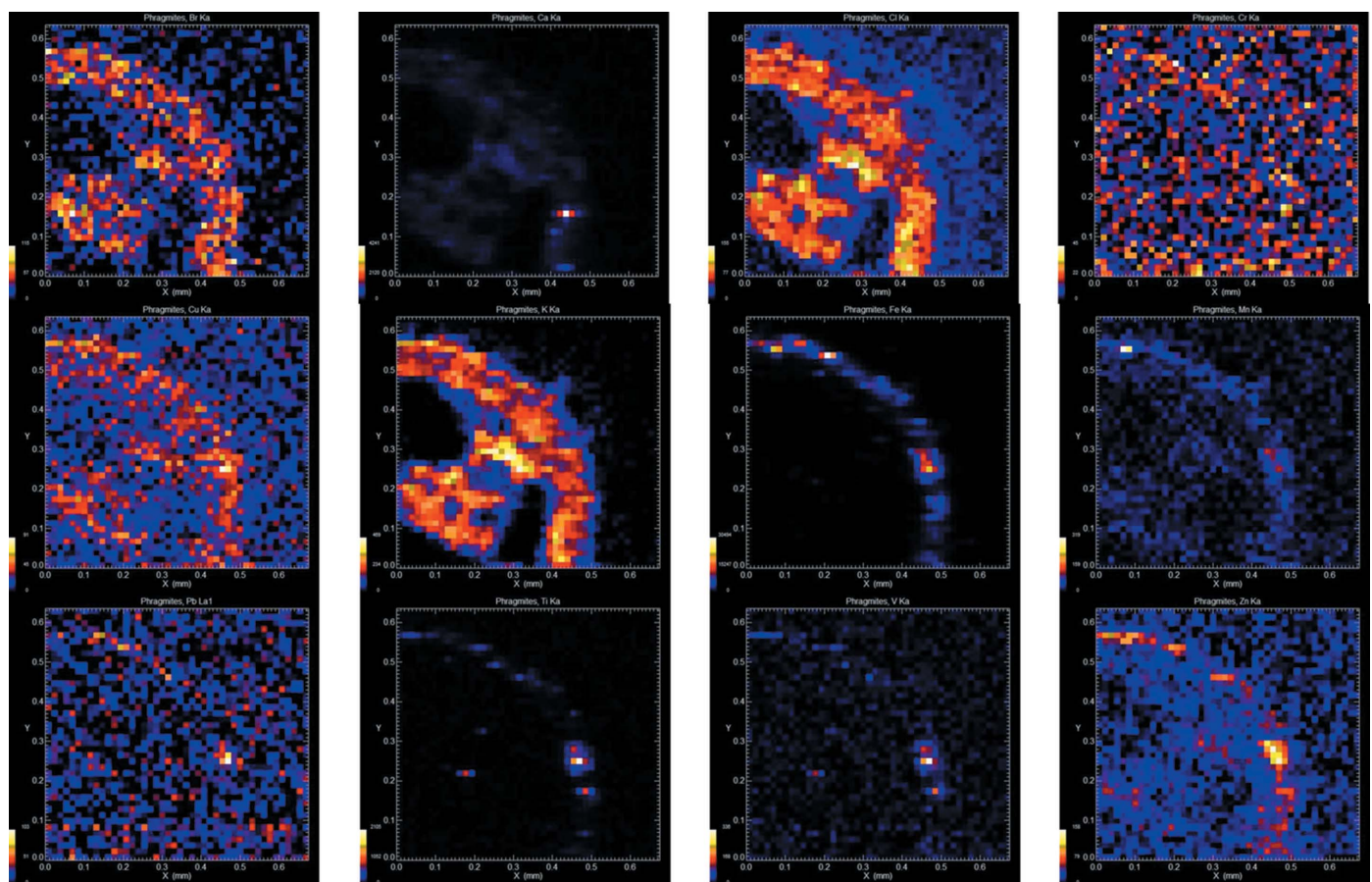


Figure 7 Metal concentrations and distributions in the root basal cross-sections of Sample 2-1, *Phragmites australis*, collected at Site 2. Top row: Br, Ca, Cl and Cr. Second row: Cu, K, Fe and Mn. Third row: Pb, Ti, V and Zn.

**Table 3**

Results of Mann-Whitney U non-parametric test and two-sample *t*-test to examine metal concentration difference between the epidermis and the vascular bundle in the root tip (Sample 1-1) and the root basal tissue (Sample 2-1), respectively. The results show that the concentration differences between the epidermis and the vascular bundle are different between the two samples.

Sample ID	Type of test	log (Br)	log (Ca)	log (Cl)	log (Cr)	log (Cu)	log (Fe)	log (K)	log (Mn)	log (Pb)	log (Ti)	log (V)	log (Zn)
Sample 1-1 at Site 1	Mann-Whitney U non-parametric test												
	<i>p</i> -value	0.000	0.000	0.000	0.033	0.000	0.000	0.000	0.000	0.152	0.000	0.109	0.000
	Two-sample <i>t</i> -test												
	<i>p</i> -value	0.000	0.000	0.000	0.013	0.000	0.000	0.000	0.000	0.323	0.000	0.019	0.000
	Bonferroni adjusted <i>p</i> -value	0.001	0.000	0.000	0.159	0.000	0.000	0.003	0.000	1.000	0.000	0.230	0.000
Dunn-Sidak adjusted <i>p</i> -value	0.001	0.000	0.000	0.148	0.000	0.000	0.003	0.000	0.991	0.000	0.207	0.000	
Sample 2-1 at Site 2	Mann-Whitney U non-parametric test												
	<i>p</i> -value	0.204	0.308	0.390	0.155	0.036	0.000	0.087	0.006	0.318	0.000	0.000	0.000
	Two-sample <i>t</i> -test												
	<i>p</i> -value	0.207	0.879	0.384	0.119	0.082	0.000	0.176	0.049	0.313	0.000	0.000	0.000
	Bonferroni adjusted <i>p</i> -value	1.000	1.000	1.000	1.000	0.986	0.000	1.000	0.585	1.000	0.000	0.000	0.001
Dunn-Sidak adjusted <i>p</i> -value	0.938	1.000	0.997	0.781	0.643	0.000	0.902	0.451	0.989	0.000	0.000	0.001	

sites and the plant tissue compositions, and performed a linear regression between the metals (Cr, Cu, Mn, Pb, V and Zn) and Fe (Fig. 8). The significant ( $p < 0.001$ ) correlations between the metals and Fe imply scavenging of these elements by the Fe nanoparticles.

#### 4. Discussion

Soil rhizosphere is a favorable environment for microbial communities and provides essential nutrients for plant growth

(Gilbert & Frenzel, 1998; Emerson *et al.*, 1999; Frenzel *et al.*, 1999; King & Garey, 1999). Plants uptake nutrients including trace metals from the rhizosphere through their root system. During the uptake and transport processes, biogeochemical processes play an important role. Metal accumulation in the epidermis of the plant roots can be predominately controlled by geochemical mechanisms such as metal adsorption/desorption at the soil/sediment-plant root interface, while high concentrations of metals in vascular bundle can be a result of symplastic or aplastic transport of these metals by their

**Table 4**

Pearson correlation matrix of elements in the epidermis and vascular bundle of the root tip. The sample was collected at Site 1. Parameters in bold face show significant correlations ( $p < 0.001$ ). The results show that most of the elements are significantly correlated in the epidermis, but not in the vascular bundle, implying similar uptake mechanisms in the epidermis, but different transport processes from the epidermis to the vascular bundle in the root tip.

Root		Br	Ca	Cl	Cr	Cu	Fe	K	Mn	Pb	Ti	V	Zn
Epidermis ( <i>n</i> = 1237)	Br	<b>1.000</b>											
	Ca	<b>0.155</b>	<b>1.000</b>										
	Cl	<b>0.580</b>	<b>0.137</b>	<b>1.000</b>									
	Cr	0.081	<b>0.285</b>	−0.002	<b>1.000</b>								
	Cu	<b>0.460</b>	<b>0.349</b>	<b>0.467</b>	<b>0.264</b>	<b>1.000</b>							
	Fe	<b>0.133</b>	<b>0.453</b>	0.093	<b>0.399</b>	<b>0.451</b>	<b>1.000</b>						
	K	<b>0.415</b>	<b>0.627</b>	<b>0.528</b>	<b>0.295</b>	<b>0.636</b>	<b>0.545</b>	<b>1.000</b>					
	Mn	<b>0.281</b>	<b>0.640</b>	<b>0.260</b>	<b>0.446</b>	<b>0.618</b>	<b>0.726</b>	<b>0.761</b>	<b>1.000</b>				
	Pb	<b>0.131</b>	<b>0.128</b>	<b>0.130</b>	<b>0.114</b>	<b>0.200</b>	<b>0.230</b>	<b>0.225</b>	<b>0.225</b>	<b>1.000</b>			
	Ti	0.090	<b>0.823</b>	0.037	<b>0.280</b>	<b>0.280</b>	<b>0.404</b>	<b>0.448</b>	<b>0.484</b>	<b>0.122</b>	<b>1.000</b>		
	V	<b>0.089</b>	<b>0.820</b>	0.035	<b>0.288</b>	<b>0.289</b>	<b>0.402</b>	<b>0.458</b>	<b>0.503</b>	<b>0.124</b>	<b>0.985</b>	<b>1.000</b>	
	Zn	<b>0.272</b>	<b>0.524</b>	<b>0.233</b>	<b>0.425</b>	<b>0.633</b>	<b>0.744</b>	<b>0.719</b>	<b>0.867</b>	<b>0.203</b>	<b>0.443</b>	<b>0.462</b>	<b>1.000</b>
	Vascular bundle ( <i>n</i> = 568)	Br	<b>1.000</b>										
Ca		<b>0.290</b>	<b>1.000</b>										
Cl		<b>0.510</b>	<b>0.569</b>	<b>1.000</b>									
Cr		0.047	−0.002	0.057	<b>1.000</b>								
Cu		<b>0.335</b>	<b>0.387</b>	<b>0.538</b>	0.038	<b>1.000</b>							
Fe		<b>0.182</b>	<b>0.313</b>	<b>0.405</b>	−0.008	<b>0.308</b>	<b>1.000</b>						
K		<b>0.520</b>	<b>0.733</b>	<b>0.881</b>	0.057	<b>0.554</b>	<b>0.447</b>	<b>1.000</b>					
Mn		<b>0.393</b>	<b>0.695</b>	<b>0.671</b>	0.018	<b>0.483</b>	<b>0.428</b>	<b>0.798</b>	<b>1.000</b>				
Pb		−0.038	−0.027	0.028	−0.079	0.025	<b>0.148</b>	0.016	0.010	<b>1.000</b>			
Ti		0.054	0.009	−0.010	−0.082	0.021	<b>0.139</b>	−0.006	0.018	0.064	<b>1.000</b>		
V		0.021	−0.042	−0.015	0.052	−0.014	0.001	−0.030	−0.046	0.024	0.102	<b>1.000</b>	
Zn		<b>0.228</b>	<b>0.247</b>	<b>0.391</b>	−0.020	<b>0.305</b>	<b>0.245</b>	<b>0.414</b>	<b>0.355</b>	0.030	0.034	−0.047	<b>1.000</b>

Table 5

Pearson correlation matrix of elements in the epidermis and vascular bundle of the root basal tissue. The sample was collected at Site 2. Parameters in bold face show significant correlations ( $p < 0.001$ ). The results show that uptake mechanisms and transport processes of each individual element in the root basal tissue may be different.

Root		Br	Ca	Cl	Cr	Cu	Fe	K	Mn	Pb	Ti	V	Zn
Epidermis ( $n = 364$ )	Br	<b>1.00</b>											
	Ca	0.02	<b>1.00</b>										
	Cl	<b>0.29</b>	<b>0.18</b>	<b>1.00</b>									
	Cr	-0.02	-0.11	-0.03	<b>1.00</b>								
	Cu	0.10	-0.01	0.06	0.06	<b>1.00</b>							
	Fe	<b>0.20</b>	-0.04	-0.11	<b>0.27</b>	<b>0.34</b>	<b>1.00</b>						
	K	<b>0.35</b>	0.15	<b>0.57</b>	0.05	<b>0.19</b>	0.17	<b>1.00</b>					
	Mn	0.17	-0.02	-0.04	<b>0.19</b>	<b>0.23</b>	<b>0.74</b>	0.12	<b>1.00</b>				
	Pb	0.05	-0.03	-0.05	0.17	0.11	<b>0.34</b>	0.09	<b>0.20</b>	<b>1.00</b>			
	Ti	0.04	-0.03	-0.11	<b>0.21</b>	<b>0.39</b>	<b>0.53</b>	0.12	<b>0.33</b>	<b>0.26</b>	<b>1.00</b>		
	V	0.02	0.00	-0.14	0.15	<b>0.28</b>	<b>0.46</b>	0.11	<b>0.31</b>	<b>0.24</b>	<b>0.86</b>	<b>1.00</b>	
	Zn	<b>0.18</b>	0.02	0.03	<b>0.20</b>	<b>0.35</b>	<b>0.66</b>	<b>0.24</b>	<b>0.53</b>	<b>0.32</b>	<b>0.51</b>	<b>0.44</b>	<b>1.00</b>
	Vascular bundle ( $n = 174$ )	Br	<b>1.000</b>										
Ca		<b>0.326</b>	<b>1.000</b>										
Cl		<b>0.360</b>	<b>0.557</b>	<b>1.000</b>									
Cr		0.025	0.048	-0.008	<b>1.000</b>								
Cu		<b>0.352</b>	<b>0.343</b>	<b>0.309</b>	0.011	<b>1.000</b>							
Fe		-0.012	0.060	0.045	0.032	-0.094	<b>1.000</b>						
K		<b>0.447</b>	<b>0.784</b>	<b>0.745</b>	-0.009	<b>0.457</b>	0.112	<b>1.000</b>					
Mn		0.240	0.186	<b>0.296</b>	0.081	<b>0.265</b>	0.003	0.207	<b>1.000</b>				
Pb		0.199	0.112	0.080	0.075	0.205	0.199	0.098	0.118	<b>1.000</b>			
Ti		-0.025	-0.077	-0.021	0.068	-0.106	<b>0.834</b>	-0.003	-0.031	0.166	<b>1.000</b>		
V		-0.067	0.055	0.014	-0.003	-0.113	<b>0.629</b>	0.037	-0.012	0.215	<b>0.742</b>	<b>1.000</b>	
Zn		<b>0.391</b>	0.239	<b>0.263</b>	0.024	0.233	-0.003	<b>0.312</b>	0.049	0.027	-0.041	-0.023	<b>1.000</b>

transport proteins. In metal uptake and transport through the roots, there are differences between the essential nutrients (e.g. Ca, Cu and Zn) and non-essential nutrients (e.g. Cr and Pb) (Feng *et al.*, 2015, 2016; Qian *et al.*, 2015). The defensive nature of the plants will not actively uptake and translocate non-essential metal nutrients to the root vascular tissues in a large quantity. In this study, synchrotron XRF micro-scale measurement demonstrated its unique role in showing high concentrations of Ca, Cu, Fe, Mn and Zn in the root system. As essential nutrients for the plant growth, these elements can be taken up, transported and accumulated in both epidermis and vascular bundle. In contrast, the results from this study show that *Phragmites australis* does not actively uptake Cr and Pb from rhizosphere soil and translocate Pb and Cr within the plant tissues (Table 1).

Although Fe is a nutrient for the plant growth, it shows a relatively high concentration in the epidermis, which can be attributed to the formation of Fe oxides due to redox reaction at the soil/sediment–root interface in the rhizosphere (Al-Sid-Cheikh *et al.*, 2015). In a previous study, synchrotron  $\mu$ XANES measurement indicates that Fe speciation in *Typha latifolia* root epidermis was dominated by Fe<sup>3+</sup> (Feng *et al.*, 2013). In this study, our synchrotron XANES measurement indicates that small Fe oxide particles, or Fe nanoparticles, appear in the root epidermis (Fig. 5). These Fe nanoparticles can be Fe-containing minerals and provide a reactive substrate to scavenge metals (Bargar *et al.*, 1997; Hansel *et al.*, 2001; Li *et al.*, 2015; Fuente *et al.*, 2016; Feng *et al.*, 2013, 2015, 2016). Several early studies suggest that the Fe plaque on the surface of roots serves as a barrier preventing heavy metals from entering plant roots (St-Cyr & Campbell, 1996; Bjørn *et al.*,

1998). However, others suggest that Fe plaque is not the main barrier (Ye *et al.*, 1998; Liu *et al.*, 2004). In this study, significant correlations of trace metals (e.g. Cr, Cu, Mn, Pb, V and Zn) with Fe in the root system suggest that Fe nanoparticles can play a significant role in scavenging trace metals in the epidermis (Tables 4 and 5, Fig. 8), although the mechanisms controlling the metal uptake, transport and accumulation in the root could be metal-dependent associated with different transport proteins. Because of the high adsorption capacity of Fe oxides and large specific surface area (Bargar *et al.*, 1997; Eick *et al.*, 1999; Otte *et al.*, 1989, 1991; Hansel *et al.*, 2001, 2002; St-Cyr & Crowder, 1990), Fe nanoparticles can provide a reactive substrate to scavenge metals for metal sequestration (Rodríguez *et al.*, 2005; Pardha-Saradhi *et al.*, 2014; Fuente *et al.*, 2016). Therefore, it is important to understand the function of Fe nanoparticles in controlling the mobility of metals in the plants. This study shows that the correlations of metals with Fe in the vascular bundle are relatively less significant than that in the epidermis (Tables 4 and 5). The metal uptake mechanisms by the roots and transport pathways within the plant tissues can be different among different metals, plant species and metal concentrations in soils/sediments (Gallagher *et al.*, 2008; Qian *et al.*, 2012, 2015; Lyubenova *et al.*, 2013; Tripathi *et al.*, 2014; Feng *et al.*, 2015, 2016). The results from this study suggest that, after the metal uptake by *Phragmites australis* from the soil, transport of metals from the epidermis to the vascular tissue and accumulation in the *Phragmites australis* root system can vary from metal to metal, most likely due to differential expression of a number of different accumulation systems (Assunção *et al.*, 2008). In other words, the mechanisms and processes controlling metal transport and distribu-

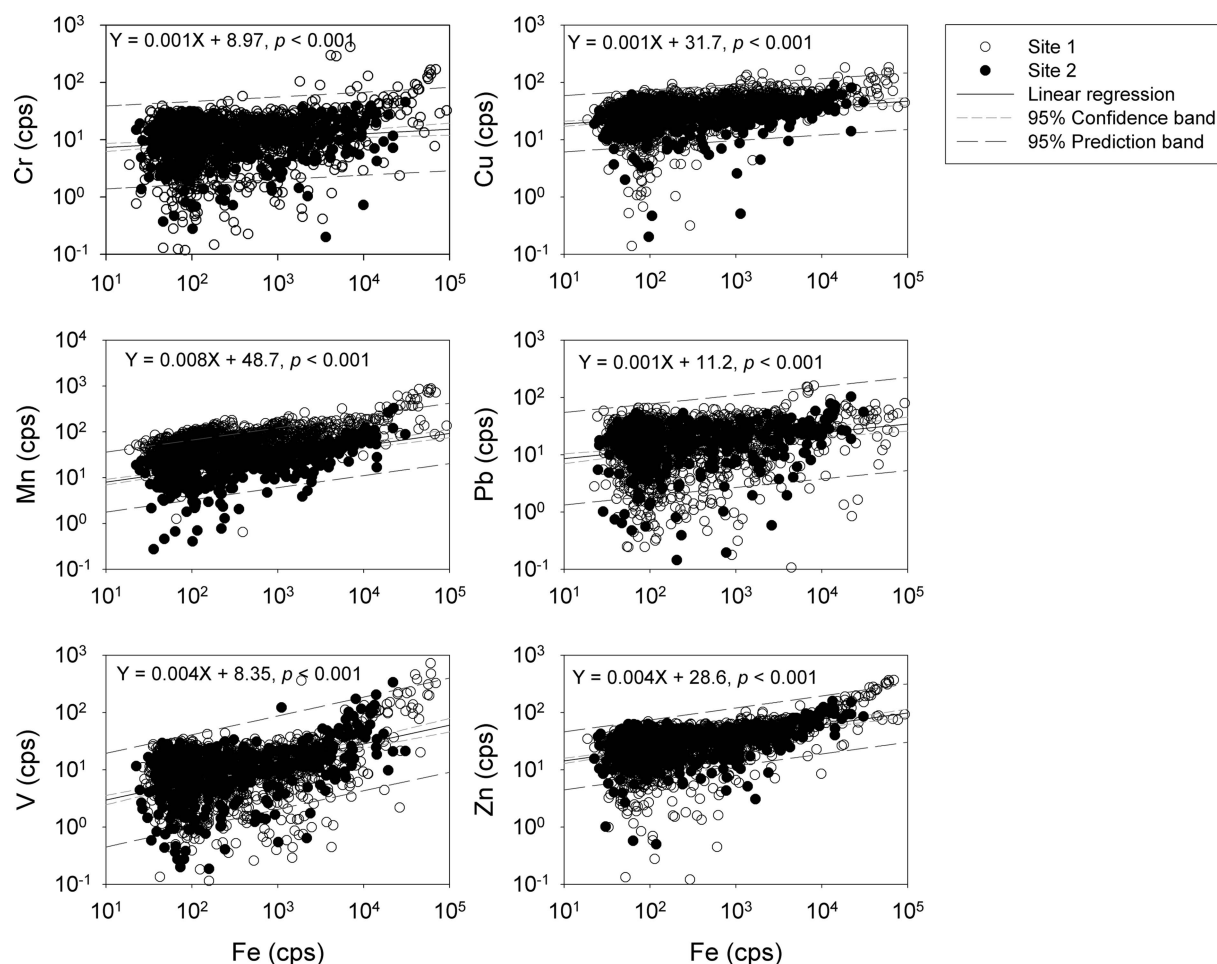


**Figure 8**  
Results of the linear regression between metals (Cr, Cu, Mn, Pb, V and Zn) and Fe in the *Phragmites australis* root samples collected at Sites 1 and 2.

tions between the epidermis and the vascular bundle in *Phragmites australis* could be different.

## 5. Conclusion

Synchrotron X-ray radiation measurement can provide new insights into the mechanisms taking place in plants during the course of metal uptake from the soils/sediments and transport in the plants at levels where interactions can be understood. This study investigates the concentrations and distributions of Br, Ca, Cl, Cr, Cu, K, Fe, Mn, Pb, Ti, V and Zn in *Phragmites australis* root system with micrometer-scale resolution in order to understand the chemical mechanisms of metal uptake by plants and the transport pathways in the plants. The results are important to understand the metal biogeochemical cycle and ecological function of the wetlands. As a complex biogeochemical process, the results show that the root epidermis can be an important environment that regulates metal biogeochemical cycling by forming less mobile metal-mineral species and metal complexes in the rhizosphere. Although this research concentrates on basic research, its outcomes have a potential application in the potential low-cost remediation effort (e.g. phytostabilization) to manage metal-contaminated sediments while performing wetland rehabilitation.

## Acknowledgements

We would like to thank Dr S. M. Heald (Co-editor of *Journal of Synchrotron Radiation*), Dr A. Weight (Managing Editor of *Journal of Synchrotron Radiation*) and two anonymous reviewers for their constructive comments and suggestions which have improved the quality of an early version of this manuscript. This work was supported in part by the State Key Laboratory of Estuarine and Coastal Research Open Research Fund (SKLEC-KF201304) (HF, WZ, LY, WL, YQ), the China Scholarship Council (YQ), and the Margaret and Herman Sokol Foundation (HF). This project was also supported in part by the US Department of Energy, Office of Science, Office of Workforce Development for Teachers and Scientists (WDTS) under the Visiting Faculty Program (VFP) (HF). Use of the NSLS was supported by the US Department of Energy, Office of Science, Office of Basic Energy Sciences, under Contract No. DE-AC02-98CH10886. NSLS X27A was supported in part by the US Department of Energy – Geosciences (DE-FG02-92ER14244 to The University of Chicago – CARS). This research used resources of the Advanced Photon Source, a US Department of Energy (DOE) Office of Science User Facility operated for the DOE Office of Science by Argonne National Laboratory under Contract No. DE-

AC02-06CH11357. Use of APS beamline 8BM is partially supported by the National Synchrotron Light Source II, Brookhaven National Laboratory, under DOE Contract No. DE-SC0012704. The part of work carried out at Biology Department, Brookhaven National Laboratory, was supported in part by the National Science Foundation through grant MCB-1051675 and by the Division of Chemical Sciences, Geosciences and Biosciences, Office of Basic Energy Sciences of the US Department of Energy through Grant DEAC0298CH10886 to CJL.

## References

- Ablett, J., Kao, C., Reeder, R., Tang, Y. & Lanzirrotti, A. (2006). *Nucl. Instrum. Methods Phys. Res. A*, **562**, 487–494.
- Al-Sid-Cheikh, M., Pédrot, M., Dia, A., Guenet, H., Vantelon, D., Davranche, M., Gruau, G. & Delhaye, T. (2015). *Sci. Total Environ.* **515–516**, 118–128.
- Assunção, A. G., Bleeker, P., ten Bookum, W. M., Vooijs, R. & Schat, H. (2008). *Plant Soil*, **303**, 289–299.
- Bargar, J., Brown, G. & Parks, G. (1997). *Geochim. Cosmochim. Acta*, **61**, 2617–2637.
- Bjørn, S., Carlos, V., Zsabel, C., Ferno, C., Maria-João, M. & Miguel, C. (1998). *Limnol. Oceanogr.* **43**, 245–252.
- Eick, M. J., Peak, J. D., Brady, P. V. & Pesek, J. D. (1999). *Soil Sci.* **164**, 28–39.
- Emerson, D., Weiss, J. V. & Megonigal, J. P. (1999). *Appl. Environ. Microbiol.* **65**, 2758–2761.
- Enstone, D. E., Peterson, C. A. & Ma, F. (2002). *J. Plant Growth Regul.* **21**, 335–351.
- Feng, H., Qian, Y., Gallagher, F. J., Wu, M., Zhang, W., Yu, L., Zhu, Q., Zhang, K., Liu, C.-J. & Tappero, R. (2013). *Environ. Sci. Pollut. Res.* **20**, 3743–3750.
- Feng, H., Qian, Y., Gallagher, F. J., Zhang, W., Yu, L., Liu, C., Jones, K. W. & Tappero, R. (2016). *J. Environ. Sci.* **41**, 172–182.
- Feng, H., Zhang, W., Liu, W., Yu, L., Qian, Y., Wang, J., Wang, J.-J., Eng, C., Liu, C.-J., Jones, K. W. & Tappero, R. (2015). *Environ. Sci. Pollut. Res.* **22**, 18933–18944.
- Frenzel, P., Bosse, U. & Janssen, P. H. (1999). *Soil Biol. Biochem.* **31**, 421–430.
- Fuente, V., Rufo, L., Juárez, B., Menéndez, N., García-Hernández, M., Salas-Colera, E. & Espinosa, A. (2016). *J. Struct. Biol.* **193**, 23–32.
- Gallagher, F. J., Pechmann, I., Bogden, J. D., Grabosky, J. & Weis, P. (2008). *Environ. Pollut.* **153**, 351–361.
- Gilbert, B. & Frenzel, P. (1998). *Soil Biol. Biochem.* **30**, 1903–1916.
- Hansel, C. M., Fendorf, S., Sutton, S. & Newville, M. (2001). *Environ. Sci. Technol.* **35**, 3863–3868.
- Hansel, C. M., La Force, M. J., Fendorf, S. & Sutton, S. (2002). *Environ. Sci. Technol.* **36**, 1988–1994.
- Hinsinger, P. & Courchesne, F. (2008). *Biophysic Chemical Processes of Heavy Metals and Metalloids in Soil Environments*, pp. 267–311. Hoboken: Wiley.
- King, G. & Garey, M. A. (1999). *Appl. Environ. Microbiol.* **65**, 4393–4398.
- Li, Y.-F., Zhao, J., Qu, Y., Gao, Y., Guo, Z., Liu, Z., Zhao, Y. & Chen, C. (2015). *Nanomed. Nanotechnol. Biol. Med.* **11**, 1531–1549.
- Liu, W., Zhu, Y., Smith, F. & Smith, S. (2004). *J. Exp. Bot.* **55**, 1707–1713.
- Lyubenova, L., Pongrac, P., Vogel-Mikuš, K., Mezek, G. K., Vavpetič, P., Grlj, N., Regvar, M., Pelicon, P. & Schröder, P. (2013). *J. Hazard. Mater.* **248–249**, 371–378.
- Martin, R. R., Naftel, S. J., Macfie, S. M., Jones, K. W., Feng, H. & Trembley, C. (2006). *X-ray Spectrom.* **35**, 57–62.
- Martin, R., Sham, T., Wong Won, G., Jones, K. & Feng, H. (2001). *X-ray Spectrom.* **30**, 338–341.
- Morrissey, J. & Guerinot, M. L. (2009). *Chem. Rev.* **109**, 4553–4567.
- Naftel, S., Martin, R., Jones, K., Feng, H., Savard, M. & Begin, C. (2001). *Can. J. Anal. Sci. Spectrosc.* **46**, 118–122.
- Otte, M., Dekkers, I., Rozema, J. & Broekman, R. (1991). *Can. J. Bot.* **69**, 2670–2677.
- Otte, M., Rozema, J., Koster, L., Haarsma, M. & Broekman, R. (1989). *New Phytol.* **111**, 309–317.
- Pardha-Saradhi, P., Yamal, G., Peddisetty, T., Sharmila, P., Singh, J., Nagarajan, R. & Rao, K. (2014). *Biometals*, **27**, 97–114.
- Qian, Y., Feng, H., Gallagher, F. J., Zhu, Q., Wu, M., Liu, C.-J., Jones, K. W. & Tappero, R. V. (2015). *J. Synchrotron Rad.* **22**, 1459–1468.
- Qian, Y., Gallagher, F. J., Feng, H. & Wu, M. (2012). *Environ. Pollut.* **166**, 23–30.
- Rodríguez, N., Menéndez, N., Tornero, J., Amils, R. & de la Fuente, V. (2005). *New Phytol.* **165**, 781–789.
- Rouff, A. A., Eaton, T. T. & Lanzirrotti, A. (2013). *Chemosphere*, **93**, 2159–2164.
- St-Cyr, L. & Campbell, P. G. (1996). *Biogeochemistry*, **33**, 45–76.
- St-Cyr, L. & Crowder, A. (1990). *Soil Sci.* **149**, 191–198.
- Sutton, S. R., Bertsch, P. M., Newville, M., Rivers, M., Lanzirrotti, A. & Eng, P. (2002). *Rev. Mineral. Geochem.* **49**, 429–483.
- Tripathi, R. D., Tripathi, P., Dwivedi, S., Kumar, A., Mishra, A., Chauhan, P. S., Norton, G. J. & Nautiyal, C. S. (2014). *Metallomics*, **6**, 1789–1800.
- Wang, J., Chen-Wiegart, Y. & Wang, J. (2014a). *Angew. Chem. Int. Ed.* **53**, 4460–4464.
- Wang, J., Chen-Wiegart, Y. & Wang, J. (2014b). *Nat. Commun.* **5**, 4570.
- Wang, J., Karen Chen, Y. C., Yuan, Q., Tkachuk, A., Erdonmez, C., Hornberger, B. & Feser, M. (2012). *Appl. Phys. Lett.* **100**, 143107.
- Weis, J. S. & Weis, P. (2004). *Environ. Int.* **30**, 685–700.
- Williams, T. P., Bubb, J. M. & Lester, J. N. (1994). *Mar. Pollut. Bull.* **28**, 277–290.
- Xiqing, C. (1998). *J. Coast. Res.* **14**, 839–858.
- Ye, Z., Baker, A. J. M., Wong, M. H. & Willis, A. J. (1998). *Aquat. Bot.* **61**, 55–67.
- Zhang, W., Feng, H., Chang, J., Qu, J., Xie, H. & Yu, L. (2009). *Environ. Pollut.* **157**, 1533–1543.
- Zhang, W., Yu, L., Hutchinson, S. M., Xu, S., Chen, Z. & Gao, X. (2001). *Geomorphology*, **41**, 195–205.
- Zimmer, D., Montañó, M., Olsaker, I., Dahl, E., Berg, V., Karlsson, C., Murk, A. J., Skaare, J. U., Ropstad, E. & Verhaegen, S. (2011). *Sci. Total Environ.* **409**, 2040–2048.